Attention-Deficit/Hyperactivity Disorder Without Comorbidity Is Associated With Distinct Atypical Patterns of Cerebral Microstructural Development

Vitria Adisetiyo,[1,2]* Ali Tabesh,[3,4] Adriana Di Martino,[5] Maria F. Falangola,[3,4,6] Francisco X. Castellanos,[1,2,5,7] Jens H. Jensen,[3,4] and Joseph A. Helpern[3,4,6]

[1]Department of Radiology, Center for Biomedical Imaging, New York University School of Medicine, New York, New York

[2]Department of Physiology & Neuroscience, New York University School of Medicine, New York, New York

[3]Center for Biomedical Imaging, Medical University of South Carolina, Charleston, South Carolina

[4]Department of Radiology and Radiological Science, Medical University of South Carolina, Charleston, South Carolina

[5]Phyllis Green and Randolph Cowen Institute for Pediatric Neuroscience, Child Study Center, New York University School of Medicine, New York, New York

[6]Department of Neurosciences, Medical University of South Carolina, Charleston, South Carolina

[7]The Nathan S. Kline Institute for Psychiatric Research, Orangeburg, New York

◆━━━━━━━━━━━━━━━━━━━━━━━━━━━━━━━━━━◆

Abstract: Differential core symptoms and treatment responses are associated with the pure versus comorbid forms of attention-deficit/hyperactivity disorder (ADHD). However, comorbidity has largely been unaccounted for in neuroimaging studies of ADHD. We used diffusional kurtosis imaging to investigate gray matter (GM) and white matter (WM) microstructure of children and adolescents with ADHD ($n = 22$) compared to typically developing controls (TDC, $n = 27$) and examined whether differing developmental patterns are related to comorbidity. The ADHD group (ADHD-mixed) consisted of subgroups with and without comorbidity (ADHD-comorbid, $n = 11$; ADHD-pure, $n = 11$, respectively). Age-related changes and group differences in cerebral microstructure of the ADHD-mixed group and each ADHD subgroup were compared to TDC. Whole-brain voxel-based analyses with mean kurtosis (MK) and mean diffusivity (MD) metrics were conducted to probe GM and WM. Tract-based spatial statistics analyses of WM were performed with MK, MD, fractional anisotropy, and directional (axial, radial) kurtosis and diffusivity metrics. ADHD-pure patients lacked significant age-related changes in GM and WM microstructure that were observed globally in TDC and had significantly greater WM microstructural complexity than TDC in bilateral frontal and parietal lobes, insula, corpus callosum, and right external and internal capsules. Including ADHD patients with diverse comorbidities in analyses masked these findings. A

distinct atypical age-related trajectory and aberrant regional differences in brain microstructure were detected in ADHD without comorbidity. Our results suggest that different phenotypic manifestations of ADHD, defined by the presence or absence of comorbidity, differ in cerebral microstructural markers.
Hum Brain Mapp 35:2148–2162, 2014.   © 2013 Wiley Periodicals, Inc.

◆━━━━━━━━━━━━━━━━━━━━━━━━━━━━━━◆

INTRODUCTION

More than 66% of attention-deficit/hyperactivity disorder (ADHD) cases have diverse comorbid disorders including externalizing (e.g., oppositional defiant and conduct disorders) and internalizing disorders (e.g., anxiety and mood disorders). Different comorbid forms of ADHD and pure ADHD have been associated with distinct core symptoms, clinical outcomes, and treatment responses [Jensen et al., 2001; Newcorn et al., 2001; Rubio et al., 2011; Takeda et al., 2012]. Although the existence of distinct clinical phenotypes suggests potentially differential neural endophenotypes, most neuroimaging studies have included heterogeneous samples without specifically accounting for comorbidity.

Magnetic resonance imaging studies utilizing diffusion tensor imaging (DTI) have consistently observed atypical gray matter (GM) and white matter (WM) microstructure in ADHD across the lifespan [Ashtari et al., 2005; Bechtel et al., 2009; Cao et al., 2010; Casey et al., 2007; Chao et al., 2009; Davenport et al., 2010; de Zeeuw et al., 2011, 2012; Dramsdahl et al., 2012; Hamilton et al., 2008; Helpern et al., 2011; Kobel et al., 2010; Konrad et al., 2010, 2011; Li et al., 2010; Makris et al., 2008; Nagel et al., 2011; Pavuluri et al., 2009; Peterson et al., 2011; Qiu et al., 2011; Rusch et al., 2007; Silk et al., 2009a,b; Skranes et al., 2007; Tamm et al., 2012; Wang et al., 2012]. However, findings have been mixed, as some authors have reported lower fractional anisotropy (FA) and/or higher mean diffusivity (MD) [Ashtari et al., 2005; Bechtel et al., 2009; Cao et al., 2010; Casey et al., 2007; Chao et al., 2009; de Zeeuw et al., 2011; Dramsdahl et al., 2012; Hamilton et al., 2008; Konrad et al., 2011; Makris et al., 2008; Nagel et al., 2011; Pavuluri et al., 2009; Qiu et al., 2011; Skranes et al., 2007; Wang et al., 2012], whereas others have found higher FA and/or lower MD [Davenport et al., 2010; Kobel et al., 2010; Konrad et al., 2010; Li et al., 2010; Peterson et al., 2011; Silk et al., 2009b; Tamm et al., 2012] in ADHD compared to typically developing controls (TDC). Although discrepancies may be attributed to differences in the age ranges and brain regions examined, some of these discordant observations have been identified within similar age groups and brain regions including frontostriatal circuits [Casey et al., 2007; Davenport et al., 2010; de Zeeuw et al., 2011; Li et al., 2010; Skranes et al., 2007; Tamm et al., 2012]. Instead, whole-brain studies involving highly screened ADHD samples, either free of comorbidity or limited to the specific comorbidity of oppositional defiant disorder (ODD), have consistently reported greater FA in ADHD compared to TDC [Konrad et al., 2010; Li et al., 2010; Peterson et al., 2011; Silk et al., 2009b].

The goal of this study was to apply diffusional kurtosis imaging (DKI) to investigate age-related changes and group differences in GM and WM microstructure in the whole-brain of children and adolescents with ADHD (8–18 years old) compared to age-, sex-, and IQ-matched TDC. Specifically, we examined whether different developmental patterns of brain microstructure are observed when the ADHD group consisted of ADHD with and without comorbidity (ADHD-mixed), compared to when these two subgroups are separated (ADHD-comorbid and ADHD-pure, respectively). DKI was utilized because it provides standard diffusion measures (FA and MD) plus additional complementary metrics related to the diffusional kurtosis of the water diffusion displacement probability distribution function [Jensen and Helpern, 2003, 2010; Jensen et al., 2005; Lu et al., 2006; Wu and Cheung, 2010]. FA quantifies the diffusional anisotropy in WM, with higher values suggesting greater directional coherence in fiber bundles and MD quantifies the general magnitude of water diffusion in tissue, with lower values indicating more restricted diffusion [Alexander et al., 2007], although these generalizations do not apply in many brain regions [Jones et al., 2012].

Mean kurtosis (MK) quantifies the extent to which diffusion is non-Gaussian, reflecting microstructural complexity; higher MK generally reflects more complex tissue microstructure [Jensen and Helpern, 2003, 2010; Jensen et al., 2005; Lu et al., 2006; Wu and Cheung, 2010]. By accounting for the fundamental non-Gaussian property of water diffusion in biological tissue, MK yields additional information about tissue microstructure beyond what FA and MD are sensitive to [Veraart et al., 2011; Wu and Cheung, 2010]. Furthermore, MK is applicable to both GM and WM, even in tissue with crossing fibers, because unlike FA, the accuracy of its estimation does not require an anisotropic environment [Lu et al., 2006]. Several preliminary DKI studies in humans and animals have shown promising results in characterizing neural microstructure in typical development [Cheung et al., 2009; Falangola et al., 2008] and pathology [Blockx et al., 2012a,2012b; Cheung et al., 2012; Gao et al., 2012; Grinberg et al., 2012; Grossman et al., 2011; Helpern et al., 2011; Hui et al., 2012; Jensen et al., 2011; Raab et al., 2010; Rosenkrantz et al., 2012; Van Cauter et al., 2012; Wang et al., 2011; Zhuo et al., 2012].

Whole-brain voxel-based analyses (VBA) with anisotropy-independent MK and MD metrics were used to probe GM and WM microstructure, whereas specific WM analyses using MK, MD, FA, and the directional metrics axial kurtosis ($K_{||}$), radial kurtosis ($K_\perp$), axial diffusivity ($D_{||}$), and radial diffusivity ($D_\perp$) were conducted with tract-based spatial statistics (TBSS). Axial metrics are sensitive to diffusion parallel to axonal fiber bundles and are believed to be influenced by axonal integrity/organization, whereas radial metrics are sensitive to diffusion perpendicular to axonal fiber bundles and are believed to be influenced by myelin integrity [Song et al., 2002; Wu and Cheung, 2010]. To our knowledge, this is the first study to address the potential confounding effects of comorbidity in the investigation of cerebral microstructure in ADHD.

MATERIALS AND METHODS

Participant Inclusion and Exclusion Criteria

Twenty-two individuals with ADHD and 27 TDC between ages 8 and 18 years old were recruited from the NYU Child Study Center, the NYU Langone Medical Center, and the local community. Demographic and diagnostic information are summarized in Table I. Parent and child informed consent and assent, respectively, were obtained as approved by the NYU School of Medicine Institutional Review Board. An estimated full-scale IQ > 79 measured with the Wechsler Abbreviated Scale of Intelligence (WASI) [Wechsler, 1999], right-handedness measured with the Edinburgh Handedness Inventory [Oldfield, 1971] and the absence of known neurological, cognitive, or chronic medical diseases were required of all subjects. The Diagnostic and Statistical Manual of Mental Disorders Text Revision (fourth edition; DSM-IV-TR) [American Psychiatric Association, 2000] diagnosis of ADHD was assessed by licensed clinicians or supervised trainees based on the Schedule of Affective Disorders and Schizophrenia for Children—Present and Lifetime Version (K-SADS-PL) [Kaufman et al., 1997] administered to each parent and child. Additionally, DSM-IV Total index of the Conners' Parent and Teacher Rating Scale—Revised: Long Version (CPRS-R: L; CTRS-R: L) [Conners, 1997a/b] were above 1.5 standard deviation (SD) beyond the mean. The Behavioral Rating Inventory of Executive Function—Parent Version (BRIEF) [Gioia et al., 2000] T-scores were ≥65. Inclusion required diagnosis of combined type ADHD or predominantly inattentive type ADHD with past DSM-IV combined type diagnosis in childhood. Diagnosis of psychotic, major depressive, conduct, tic, or pervasive developmental disorders was exclusionary. Inclusion as a TDC required absence of any Axis I disorder, except for specific phobia, based on the K-SADS-PL and T-scores ≤ 65 on the CPRS-R: L DSM-IV indices and Conners' Global Index.

Image Acquisition

Participants were scanned at 3T (TIM Trio, Siemens Medical Solutions, Erlangen, Germany) with a transmission body coil and an eight-element phased array coil for reception. Whole-brain, anterior commissure–posterior commissure aligned scans were collected in a single session, with the following pulse sequences: (1) T1-weighted magnetization-prepared rapid gradient echo images with repetition time (TR) between 180° inversion pulses = 2,200 ms, echo time (TE) = 2.26 ms, flip angle = 12°, 1 slab, slices per slab = 160, slice oversampling = 30%, bandwidth = 260 Hz/pixel, echo spacing = 5.5 ms, field-of-view (FOV) = 192 × 256 mm, slice thickness = 1 mm, matrix = 192 × 256 in a total time of 3 min and 29 s. (2) DKI data were acquired using a dual-spin-echo echo planar imaging (EPI) diffusion sequence with TR/TE = 6,400/96 ms, FOV = 222 × 222 mm^2, matrix = 82 × 82, parallel imaging factor = 2, oblique axial slices (number/thickness) = 49/2.7 mm without gaps, 30 diffusion encoding directions with three b-values (0, 1,000, and 2,000 s/mm^2) for each direction, two averages with nine additional b = 0 averages in a total time of 14 min and 57 s. All images were visually inspected to ensure only images free of artifacts were included in subsequent analyses. Specifically, this required the absence of motion artifacts (i.e., ghosting signal outside the head, blurred images, and/or complete loss of signal in axial slices), vibration artifacts in diffusion weighted images specific to Siemens TIM Trio scanners (i.e., localized signal drops within the head inconsistent with anatomy) [Gallichan et al., 2010] and any other artifacts that result in atypical signal inside and outside the head (e.g., single or patterned zipper artifacts and/or uneven gradient or ripples of signal intensity). As a result, 16 scans were repeated and seven were excluded. Additionally, measures of head motion were analyzed to further verify diffusion image quality (Supporting Information Methods, Supporting Information Fig. S1).

Image Processing

DKI data were processed using in-house software called Diffusional Kurtosis Estimator (www.nitrc.org/projects/dke). The diffusion and kurtosis tensors were calculated on a voxel-by-voxel basis to produce skull-stripped parametric maps for MD (μm^2/ms), $D_{||}$ (μm^2/ms), $D_\perp$ (μm^2/ms), FA (range, 0–1), MK, $K_{||}$, and $K_\perp$ (unitless) as described previously [Jensen and Helpern, 2010; Tabesh et al., 2011]. MD, $D_{||}$, $D_\perp$, and FA were calculated with b-values of 0 and 1,000 s/mm^2 that are typical for DTI, whereas kurtosis metrics MK, $K_{||}$, and $K_\perp$ were calculated with all acquired b-values. Data preprocessing with SPM8 (Statistical Parametric Mapping, Wellcome Department of Imaging Neuroscience, University College London, United Kingdom) included 3D motion correction and spatial smoothing with a Gaussian filter (3.375 mm full width at half maximum (FWHM)).

TABLE I. Demographics

	TDC (n = 27)	ADHD-mixed (n = 22)	Group Comparisons		ADHD-pure (n = 11)	ADHD-comorbid (n = 11)	Subgroup Comparisons
Comorbidity: # (no/yes)	—	11/11	—		11/0	0/11	$P^{§}$ = 1.0
Subtype: # (combined/ inattentive)	—	14/8	—		7/4	7/4	$P^{§}$ = 1.0
Medication: # (naïve/ current, past)	—	12/10	—		6/5	6/5	$P^{§}$ = 1.0
Males: # (%)	12 (44)	15 (68)	$p = 0.10^{†}$		8 (73)	7 (64)	Exact $p^{‡}$ = 0.27
	Mean (SD)	Mean (SD)	t* (df)	p-value	Mean (SD)	Mean (SD)	$F(2,46)$**, p
Age (years)	13.3 (2.6)	12.6 (2.8)	−0.8 (44)	0.40	12.9 (3.0)	12.3 (2.7)	0.50, 0.61
Age range	8.6–18.1	8.3–18.2	—	—	8.3–17.6	8.7–18.2	—
WASI							
FSIQ	111.3 (14.7)	106.8 (15.6)	−1.0 (44)	0.30	109.7 (15.9)	103.8 (15.3)	0.97, 0.39
VIQ	110.3 (14.1)	107.0 (16.1)	−0.7 (42)	0.46	109.1 (13.0)	104.9 (19.1)	0.49, 0.62
PIQ	110.6 (16.0)	105.5 (15.7)	−1.1 (45)	0.26	109.4 (18.4)	101.5 (12.1)	1.3, 0.28
CPRS-R:L			U^{a}	p < value	Mean (SD), vs. TDC p-value[b]	Mean (SD), vs. TDC p-value[b]	p-value[b]
ADHD Index	45.6 (4.4)	72.8 (11.7)	2.0	<0.001	73.1 (13.5), <0.001	72.5 (10.3), <0.001	0.92
DSM-IV Inattentive	45.7 (4.5)	73.8 (9.9)	2.0	<0.001	72.0 (9.7), <0.001	75.5 (10.2), <0.001	0.41
DSM-IV Hyperactive- Impulsive	46.5 (5.8)	67.4 (12.0)	24.0	<0.001	66.4 (12.3), <0.001	68.5 (12.2), <0.001	0.69
DSM-IV Total	45.6 (5.1)	72.2 (13.5)	30.0	<0.001	71.8 (10.8), <0.001	72.5 (16.3), <0.001	0.90
BRIEF-parent							
Behavioral Regulation Index	43.1 (7.9)	61.9 (10.1)	34.0	<0.001	58.2 (8.7), <0.001	65.6 (10.5), <0.001	0.09
Metacognition Index	44.4 (8.7)	74.6 (10.2)	3.5	<0.001	76.3 (12.7), <0.001	72.9 (7.2), <0.001	0.46
Global Executive Composite	42.9 (7.8)	71.6 (9.1)	2.0	<0.001	71.4 (10.8), <0.001	71.8 (7.5), <0.001	0.91

Group comparisons (TDC, ADHD-mixed):
[†]Pearson's χ^2 (1, N = 49) = 2.8 (two sided)
[*]Student's t-tests (two-tailed, unequal variances assumed)
[a]Mann–Whitney U-test (two-tailed). *Subgroup comparisons*:
[§]Fisher's Exact test (two-sided: ADHD-pure, ADHD-comorbid),
[‡]Exact Pearson's χ^2 (2, N = 49) = 2.9 (two-sided: TDC, ADHD-pure, ADHD-comorbid),
[**]one-way ANOVA (TDC, ADHD-pure, ADHD-comorbid)
[b]Mann–Whitney U test (two-tailed: ADHD-pure, ADHD-comorbid unless stated ADHD subgroup vs. TDC) following Kruskal–Wallis test, p < 0.001 (TDC, ADHD-pure, ADHD-comorbid).
Abbreviations: WASI, Wechsler Abbreviated Scale of Intelligence; FSIQ, full-scale IQ; VIQ, verbal IQ; PIQ, performance IQ; CPRS-R: L, Conners' Parent Rating Scale-Revised-Long version (*T*-scores); BRIEF-parent, Behavioral Rating Inventory of Executive Function—parent version (*T*-scores); DSM-IV, Diagnostic and Statistical Manual of Mental Disorders, 4th Edition; SD, standard deviation; df, degrees of freedom; —, not applicable; vs., versus.

WM TBSS Analyses

Voxel-wise analyses of WM were performed with TBSS (version 1.2) [Smith et al., 2006] running in FSL4.1.2 (FMRIB Software Library, Nuffield Department of Clinical Neurosciences, University of Oxford, United Kingdom) with statistical analyses performed only in the voxels of a WM skeleton restricted to the center of WM tracts. This approach minimizes the confounding partial volume effects that typically compromise WM-specific metrics. All parametric maps were normalized into the $1 \times 1 \times 1$ mm^3

MNI152 standardized space using FSL's FNIRT. Each subject's FA map was transformed into standard space by combining a nonlinear transform that registers the FA map to a standard target FA image with an affine transform that aligns that target image to the MNI152 space. This combined transformation was applied to all parametric maps. The WM skeleton mask was generated from the mean of all normalized FA maps (mean FA ≥0.3) from subjects involved in the particular analysis then applied to the normalized parametric maps. Permutation-based statistics were computed using the *randomise* tool (2,000 permutations) [Nichols and Holmes, 2002]. Within-group linear age regression analyses were run separately for the TDC group, ADHD-mixed group, ADHD-pure subgroup, and the ADHD-comorbid subgroup. Voxels were tested for metrics increasing or decreasing significantly with age (each direction one-tailed, age mean centered within each group). Between group analyses were conducted between TDC and ADHD cohorts (i.e., TDC vs. ADHD-mixed, TDC vs. ADHD-pure, and TDC vs. ADHD-comorbid) using Student's *t*-tests with age as a covariate (age mean centered between the two groups, variances assumed unequal). Threshold-free cluster enhancement (TFCE) [Smith and Nichols, 2009] was applied to correct for familywise error from multiple comparisons ($p < 0.05$).

Whole-Brain VBA

Whole-brain VBA of GM and WM were conducted with SPM5 for MK and MD. The same normalized maps generated from the TBSS analyses were smoothed with an $8 \times 8 \times 8$ mm^3 FWHM Gaussian kernel using the *spm_smooth* function. A brain mask without cerebral spinal fluid was generated from all normalized MD maps of subjects involved in the specific analysis. The same statistical analyses from the TBSS analyses were performed but confined to voxels within the group-specific brain mask. False discovery rate (FDR) correction was used to correct for multiple comparisons ($p < 0.05$).

For VBA and TBSS analyses, anatomical localization and regional percentages with significant clusters were based on the Johns Hopkins University ICBM-DTI-81 WM labels atlas and the MNI structural atlas masks provided in FSL.

RESULTS

Clinical Demographics

The TDC and ADHD groups did not differ statistically in age, sex distribution, IQ, or parent-identified ethnicity (Caucasian: TDC 44%, ADHD 45%; African-American: TDC 41%, ADHD 36%; Latino: TDC 7%, ADHD 18%; Other including Asian or mixed: TDC 7%, ADHD 0%; Pearson's χ^2 (3, $N = 49$) = 2.8 (two-sided), exact $p < 0.51$). Of the 22 participants with ADHD (ADHD-mixed group), half had diverse comorbid disorders (ADHD-comorbid subgroup), whereas the remaining half were comorbidity-free (ADHD-pure subgroup). The ADHD-comorbid subgroup composed of patients with anxiety not otherwise specified ($n = 2$), separation anxiety disorder ($n = 1$), dysthymic disorder ($n = 1$), nocturnal enuresis ($n = 1$), reading disorder ($n = 2$), expressive language disorder ($n = 1$), obsessive–compulsive disorder ($n = 1$), ODD ($n = 1$), and ODD + bulimia + sleep disorder ($n = 1$). The ADHD subgroups did not differ statistically in age, sex distribution, IQ, subtype, medication history, or symptom ratings. Both ADHD subgroups differed significantly in symptom ratings from TDC but not in age, sex distribution, or IQ. Table I summarizes all demographics.

VBA of Age-Related Changes in GM and WM Microstructure

Significant increases in GM and WM microstructural complexity with increasing age were detected within all cortical lobes in TDC as indexed by increasing MK (Fig. 1: left-most column; FDR $p < 0.05$, t-values = 1.91–8.21, mean = 3.14, SD = 0.82; Fig. 2: corresponding effect sizes in left-most column; FDR $p < 0.05$, r-values = 0.36–0.85, mean = 0.52, SD = 0.09) as confirmed by the MNI structural atlas masks provided in FSL. ADHD-mixed displayed similar MK increases with age albeit in more widespread regions including bilateral thalamus and corpus callosum (genu) (Fig. 1: second column from left; FDR $p < 0.05$, t-values = 1.97–9.31, mean = 3.19, SD = 0.92; Fig. 2: corresponding effect sizes in second column from left; FDR $p < 0.05$, r-values = 0.40–0.90, mean = 0.57, SD = 0.10). The age-related MK increases in ADHD-mixed were driven by nearly identical patterns in ADHD-comorbid (Fig. 1: fourth column; FDR $p < 0.05$, t-values = 2.09–26.63, mean = 3.62, SD = 1.24; Fig. 2: corresponding effect sizes in fourth column; FDR $p < 0.05$, r-values = 0.57–0.99, mean = 0.74, SD = 0.09). In contrast, the ADHD-pure subgroup did not display any voxels with significant age-related MK increases (Figs. 1 and 2: third column) except when the significance threshold was lowered (Fig. 1: right-most column; uncorrected $p < 0.001$; Fig. 2: corresponding effect sizes in right-most column; uncorrected $p < 0.001$). Even at subthreshold, voxels with age-related MK increases within the ADHD-pure subgroup were less regionally extensive compared to the other cohorts (i.e., TDC, ADHD-mixed, and ADHD-comorbid) in that MK increases were restricted to small bilateral clusters scattered in all cerebral lobes. MD detected similar age-related increases in GM and WM microstructural integrity as indexed by decreasing MD with increasing age, but less sensitively than MK (Supporting Information Figs. S2 and S3).

TBSS Analyses of Age-related Changes in WM Properties

In TDC, global increases in WM microstructural complexity were detected with increasing age, as indexed by significantly increasing MK in 70.8% of all voxels within
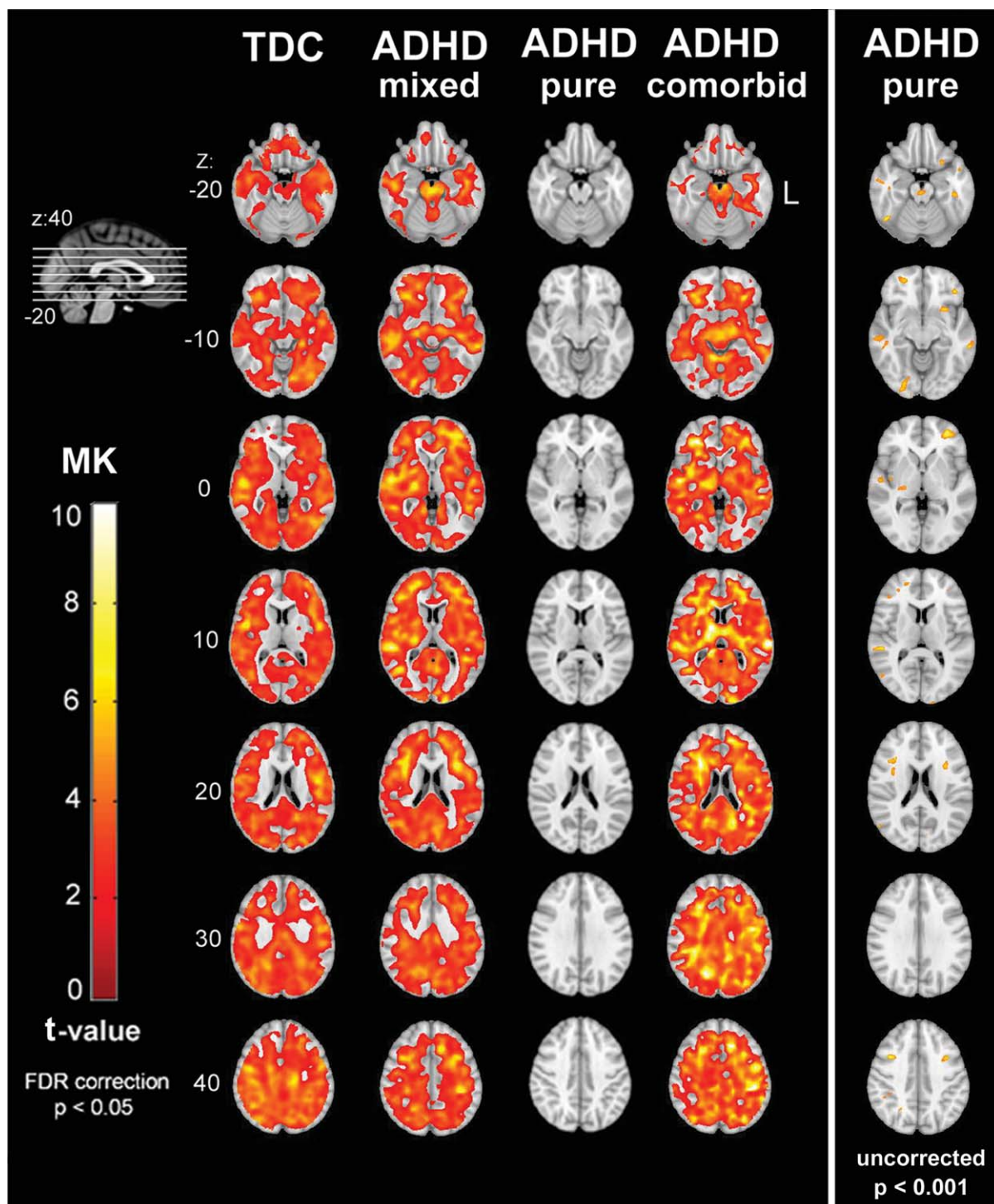
Figure 1.

Age-related increases in GM and WM microstructure indexed by increasing MK. Whole-brain VBA of MK regression with age were conducted within the TDC group (left-most column), ADHD-mixed group (second column from left), ADHD-pure subgroup (third column), and ADHD-comorbid subgroup (fourth column). Voxel-level FDR correction was applied to correct for multiple comparisons ($p < 0.05$). Only significant clusters are displayed on axial slices (red–yellow corresponding to low–high significance). For the TDC, ADHD-mixed groups and the ADHD-comorbid subgroup, MK was found to be significantly increasing with increasing age whereas the ADHD-pure subgroup displayed no significant age-related changes except when the significance threshold was lowered by removing the FDR correction (right-most column: uncorrected $p < 0.001$). All images are in radiological convention (R-right = L-left) and normalized into $1 \times 1 \times 1$ mm^3 MNI152 standard space. For the ADHD-comorbid subgroup, there were 0.15% of significant voxels with t-values above the displayed range of 0–10. For visual efficiency, these voxels were displayed as having the maximum value within the range.
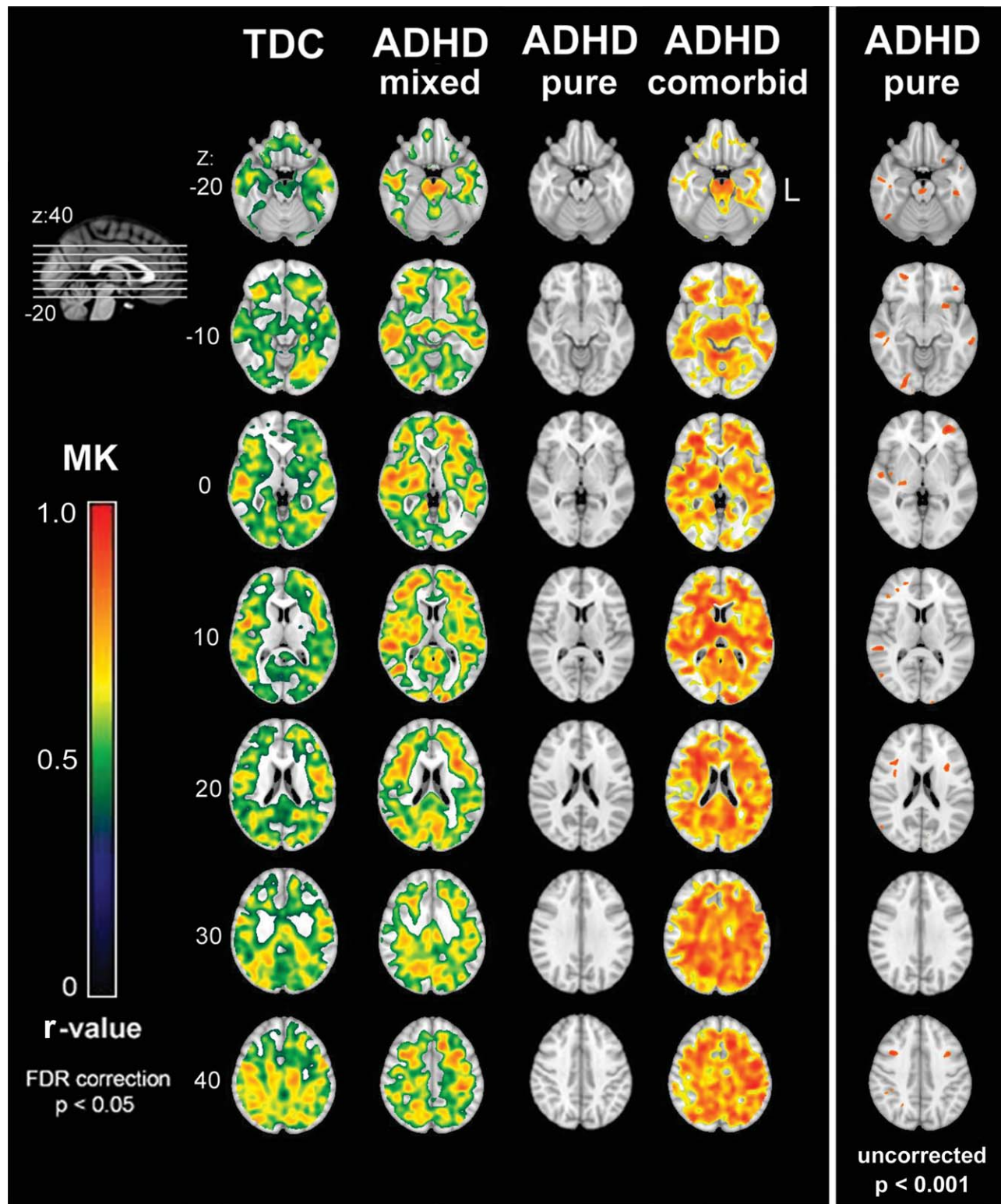
Figure 2.

Age-related increases in GM and WM microstructure indexed by increasing MK: effect sizes. Whole-brain VBA of MK regression with age were conducted within the TDC group (left-most column), ADHD-mixed group (second column from left), ADHD-pure subgroup (third column), and ADHD-comorbid subgroup (fourth column). Voxel-level FDR correction was applied to correct for multiple comparisons ($p < 0.05$). Only significant clusters are displayed on axial slices (blue–red corresponding to low–high effect sizes: correlation coefficient r-values). For the TDC, ADHD-mixed groups, and the ADHD-comorbid subgroup, MK was found to be significantly increasing with increasing age whereas the ADHD-pure subgroup displayed no significant age-related changes except when the significance threshold was lowered by removing the FDR correction (right-most column: uncorrected, $p < 0.001$). All images are in radiological convention (R-right = L-left) and normalized into $1 \times 1 \times 1$ mm^3 MNI152 standard space.
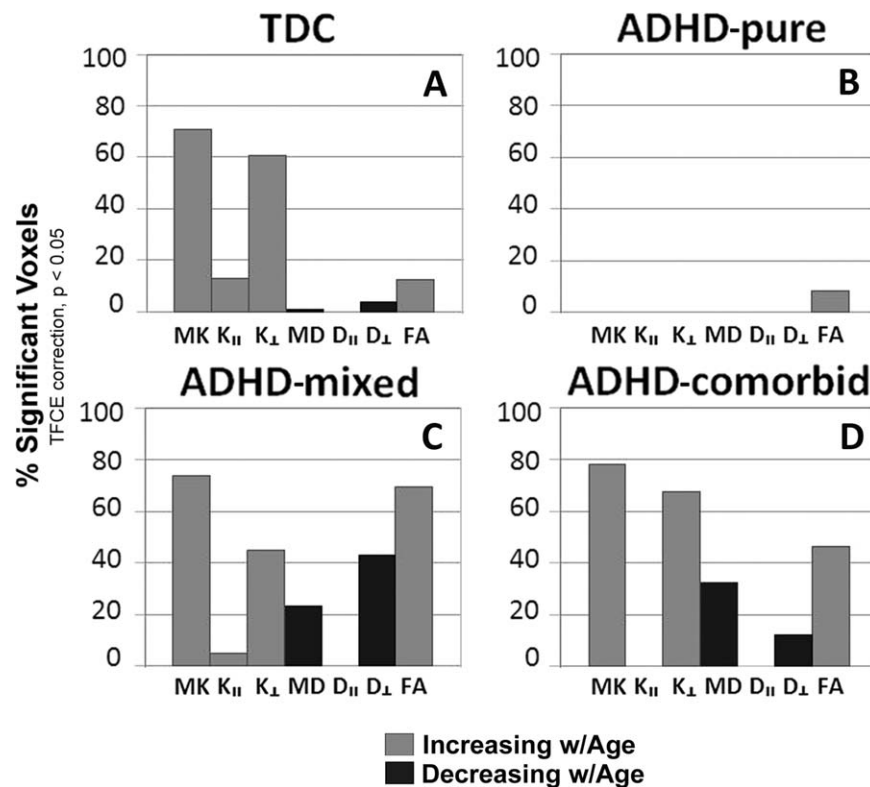
Figure 3.

Percent of WM voxels with significant age-related changes in microstructure. WM TBSS analyses of metric regression with age were conducted within the (**A**) TDC group, (**C**) ADHD-mixed group, (**B**) ADHD-pure subgroup, and (**D**) ADHD-comorbid subgroup. For each group and subgroup, MK, $K_{||}$, $K_{\perp}$, MD, $D_{||}$, $D_{\perp}$, and FA metrics were tested for significant increases or decreases with increasing age. Voxel-level TFCE correction for familywise error was applied with 2,000 permutations to correct for multiple comparisons ($p < 0.05$). The percent of significant voxels within the WM skeleton mask is displayed for each metric within each group and subgroup.

the TBSS WM skeleton mask (TFCE $p < 0.05$). Directional kurtosis metrics revealed that these MK increases in WM were mainly owing to kurtosis increases in the radial direction rather than the axial direction ($K_{\perp} = 60.8\%$ vs. $K_{||} = 12.8\%$ significant voxels at TFCE $p < 0.05$; Fig. 3A; Supporting Information Fig. S4: first top row). ADHD-mixed displayed age-related WM kurtosis patterns resembling the TDC (MK = 73.8%, $K_{||} = 4.9\%$, $K_{\perp} = 45.0\%$ significant voxels at TFCE $p < 0.05$; Fig. 3C; Supporting Information Fig. S4: second row). These patterns were repeated in the ADHD-comorbid subgroup (MK = 78.3%, $K_{||} = 0\%$, $K_{\perp} = 67.5\%$ significant voxels at TFCE $p < 0.05$; Fig. 3D; Supporting Information Fig. S4: fourth row) but not in the ADHD-pure subgroup. No significant kurtosis changes were observed in ADHD-pure (Fig. 3B; Supporting Information Fig. S4: third row).

Diffusivity metrics detected comparable age-related increases in WM microstructural integrity as indexed by decreasing MD and $D_{\perp}$ in TDC (MD = 0.9%, $D_{||} = 0\%$, $D_{\perp} = 3.6\%$ significant voxels at TFCE $p < 0.05$; Fig. 3A; Supporting Information Fig. S5: first top row), ADHD-mixed (MD = 23.5%, $D_{||} = 0\%$, $D_{\perp} = 43.1\%$ significant voxels at TFCE $p < 0.05$; Fig. 3C; Supporting Information Fig. S5: second row) and ADHD-comorbid (MD = 32.6%, $D_{||} = 0.2\%$, $D_{\perp} = 12.3\%$ significant voxels at TFCE $p < 0.05$, Fig. 3D; Supporting Information Fig. S5: fourth row). No significant diffusivity changes were found in the ADHD-pure subgroup (Fig. 3B; Supporting Information Fig. S5: third row). Significant increases in FA were observed in all cohorts to varying degrees (TDC = 12.4%; ADHD-mixed = 69.6%; ADHD-pure = 8.6%; ADHD-comorbid = 46.5% significant voxels at TFCE $p < 0.05$; Fig. 3; Supporting Information Fig. S6).

VBA and TBSS Analyses of Regional Group Differences

VBA of GM did not reveal any significant MK or MD differences between TDC and the different ADHD cohorts

(i.e., TDC vs. ADHD-mixed, TDC vs. ADHD-pure, and TDC vs. ADHD-comorbid) (FDR $p > 0.05$). Significant group differences in WM were detected with TBSS. Compared to TDC, ADHD-mixed had greater WM microstructural complexity as indexed by significantly higher MK in dorsal frontal lobes (superior longitudinal fasciculus-SLF, anterior and superior corona radiata), parietal lobes (SLF, superior and posterior corona radiata, left cingulate, left posterior thalamic radiations including optic radiations-PTR), temporal lobes (sagittal striata including the inferior longitudinal fasciculus and inferior fronto-occipital fasciculus, left PTR), left occipital lobe (SLF, PTR), right brainstem, thalamus, insula (SLF, right anterior corona radiata), external capsules, internal capsules (posterior and retrolenticular limbs) and corpus callosum (genu, body, splenium) (Fig. 4A: first left column, orange and maroon clusters; TFCE $p < 0.05$, t-values = 1.41–4.85, mean = 2.20, SD = 0.56; d-values = 0.41–1.42, mean = 0.64, SD = 0.16). ADHD-mixed also had greater tissue microstructural complexity as indexed by significantly higher $K_{||}$ in ventral and dorsal frontal lobes (SLF, anterior and superior corona radiata, left cingulate), parietal lobes (right SLF, superior and posterior corona radiata, left cingulate, left PTR), temporal lobes (sagittal striata, left PTR), left occipital lobe (SLF, posterior corona radiata), left brainstem, left thalamus, insula (anterior corona radiata, right SLF), external capsules, internal capsules (retrolenticular, right anterior and left posterior limbs), and corpus callosum (genu, body, splenium) (Fig. 4A: first left column, blue and maroon clusters; TFCE $p < 0.05$, t-values = 1.12–4.32, mean = 1.79, SD = 0.47; d-values = 0.33–1.27, mean = 0.53, SD = 0.14).

ADHD subgroup analyses revealed that clusters with higher MK observed in ADHD-mixed were detected only in ADHD-comorbid (Fig. 4A: third column, orange clusters; TFCE $p < 0.05$, t-values = 1.36–4.51, mean = 2.02, SD = 0.51; d-values = 0.50–1.66, mean = 0.74, SD = 0.19): frontal lobes (SLF, left anterior and superior corona radiata, left cingulate), parietal lobes (SLF, superior and posterior corona radiata, cingulate, PTR), right temporal lobe (sagittal striata, SLF), left occipital lobe (SLF, PTR), brainstem, thalamus, insula (SLF, superior corona radiata, left anterior corona radiata), right external capsule, internal capsule (posterior and retrolenticular limbs, left anterior limb), and corpus callosum (genu, body, splenium). The higher $K_{||}$ clusters in ADHD-mixed were detected only in ADHD-pure (Fig. 4A: middle column, blue clusters; TFCE $p < 0.05$, t-values = 1.36–6.48, mean = 2.24, SD = 0.69; d-values = 0.50–2.38, mean = 0.82, SD = 0.26): frontal lobes (SLF, anterior and superior corona radiata, right cingulate), parietal lobes (SLF, superior corona radiata, right posterior corona radiata, right cingulate), insula (anterior corona radiata, right SLF), right external capsule, right internal capsule (anterior limb), and the corpus callosum (genu, body, splenium).

Diffusivity metrics suggested greater WM microstructural integrity in ADHD-mixed compared to TDC as indexed by significantly lower MD: right frontal lobe (SLF, superior corona radiata), right parietal lobe (SLF, superior and posterior corona radiata), and right insula (SLF) (Fig. 4B: first left column, magenta clusters; TFCE $p < 0.05$, t-values = 2.22–4.44, mean = 2.72, SD = 0.42; d-values = 0.65–1.30, mean = 0.80, SD = 0.12). ADHD subgroup analyses found that all clusters with significantly lower MD in ADHD-mixed (excluding right posterior corona radiata in the parietal lobe) were detected only in ADHD-pure (Fig. 4B: middle column, magenta clusters; TFCE $p < 0.05$, t-values = 2.57–4.67, mean = 3.06, SD = 0.37; d-values = 0.94–1.72, mean = 1.12, SD = 0.14). No significant group and subgroup differences were observed with FA. Supporting Information Table S1 summarizes the anatomical localization of all significant group differences.

DISCUSSION

Converging lines of evidence suggest that pure ADHD and comorbid forms of ADHD differ in treatment response and possibly in neural endophenotypes [Jensen et al., 2001; Newcorn et al., 2001; Rubio et al., 2011; Sauder et al., 2012; Takeda et al., 2012]. By differentiating ADHD subgroups based on comorbidity and utilizing comprehensive DKI-based diffusion metrics to assess tissue microstructure, we were able to detect distinct atypical age-related patterns of tissue microstructural complexity within the ADHD-pure subgroup, which were obscured when youth with ADHD and comorbid disorders were included in analyses.

Consistent with the previous studies on typical brain development, we identified significant age-related increases in GM and WM microstructural integrity and complexity from ages 8 to 18 years within all cerebral lobes in TDC [Bava et al., 2010; Falangola et al., 2008; Lebel et al., 2008. Increases in GM microstructural complexity may indicate an increase in dendrites/spines, synaptic pruning/refinement, or changes in cell packing density, whereas increases in WM microstructural complexity may reflect increased myelination, denser axon and fiber bundle packing, refined fiber organization, or changes in axonal membrane permeability [Benes et al., 1994; Huttenlocher and Dabholkar, 1997; Webster et al., 2011]. In WM, the significant increases were predominantly seen in the radial direction, consistent with myelin-related changes. This is in agreement with the high rate of myelination which characterizes this age range [Bava et al., 2010].

In contrast, the ADHD-pure subgroup lacked these significant age-related changes in tissue microstructural integrity and complexity within all cerebral lobes. This observation replicates our preliminary DKI study of the prefrontal cortex in a separate cohort of mostly comorbidity-free adolescents with ADHD [Helpern et al., 2011]. Our findings are in apparent contrast with another study in comorbidity-free ADHD of the same age range which reported significant FA increases with age from whole-
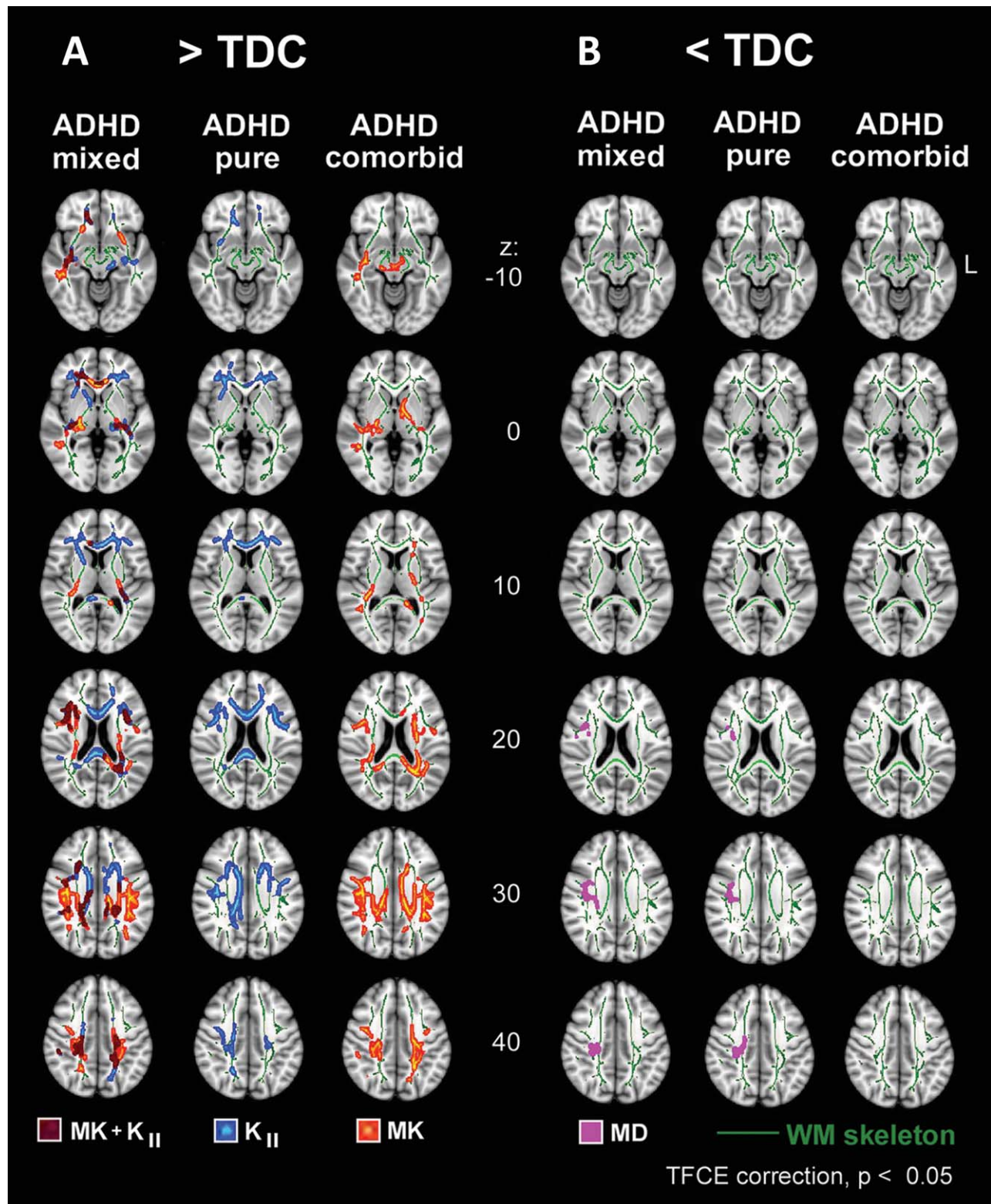
Figure 4.

Dissociable patterns of greater WM microstructure in ADHD cohorts. TBSS analyses of group means within the WM skeleton mask (green voxels) detected (**A**) significantly higher kurtosis metrics in the ADHD cohorts; first left column: ADHD-mixed > TDC in MK (orange and maroon clusters) and $K_{||}$ (blue and maroon clusters), second column: ADHD-pure > TDC in $K_{||}$ (blue clusters), third column: ADHD-comorbid > TDC in MK (orange clusters). (**B**) Significantly lower MD in the ADHD cohorts were also detected; first left column: ADHD-mixed < TDC in MD (magenta clusters), second column: ADHD-pure < TDC in MD (magenta clusters). Student's t-tests were conducted and voxel-level TFCE correction for familywise error was applied with 2,000 permutations to correct for multiple comparisons ($p < 0.05$). All images are in radiological convention (R-right = L-left), normalized into $1 \times 1 \times 1$ mm^3 MN1152 standard space and significant clusters have been thickened using the FMRIB Software Library "tbss_fill" tool for visualization.

brain and basal ganglia regions of interest [Silk et al., 2009a,b]. Methodological differences may explain this discrepancy including the use of FA, a WM specific metric, in GM regions.

Surprisingly, the stagnant age-related trajectory was unique to the ADHD-pure subgroup. Combining the ADHD patients with and without comorbidity (ADHD-mixed group) resulted in a developmental trajectory resembling TDC. Age-related patterns similar to the ADHD-mixed group were observed in the ADHD-comorbid subgroup, suggesting that their developmental trajectory was driving the age-related changes in the ADHD-mixed group. Given that ADHD patients with comorbidity have been associated with increased ADHD symptom severity and poorer outcome [Jensen et al., 2001; Newcorn et al., 2001], we did not expect age-related microstructural changes in the ADHD-comorbid subgroup to look similar to the age-related changes in TDC. However, the diversity of comorbid disorders present in our sample may account for this observation. Similar to most previous microstructural studies on ADHD, we recruited a heterogeneous ADHD sample with regard to comorbidity. However, compared to other such studies, our ADHD-comorbid sample included somewhat lower than typical rates of externalizing disorders (18%), and learning disorders (27%), and somewhat higher rates of internalizing disorders (45%), and somatic disorders (enuresis, sleep, eating; 18%). Such a broad dispersion of comorbid conditions with distinct symptom profiles makes it difficult to interpret the age-related microstructural changes observed within the ADHD-comorbid subgroup, and consequently within the ADHD-mixed group. The most likely explanation is that the global increase of tissue microstructure in the ADHD-comorbid subgroup represents a noisy mixture of multiple microstructural trajectories from various comorbid forms of ADHD. A similar loss of difference from TDC was found in corpus callosum area measurements in children with ADHD comorbid with Tourette syndrome [Baumgardner et al., 1996].

If the ADHD-pure subgroup is distinguished by a lack of significant age-related increases in tissue microstructure as seen in TDC, what can be inferred about the specific neural properties underlying this observation? After covarying for age, we found significantly greater WM microstructural complexity in the ADHD-pure subgroup relative to TDC as indexed by higher $K_{||}$ predominantly in bilateral ventral/dorsal frontal lobes, parietal lobes, insula, corpus callosum, and right external and internal capsules. To a lesser degree, lower MD within similar regions in the right hemisphere reflected more restricted diffusion in the WM, as is expected with greater tissue microstructural complexity. These frontoparietal regions have been implicated in the attention, working memory, and inhibition deficits of ADHD [Konrad and Eickhoff, 2010], but greater microstructural complexity in these regions may consistently characterize comorbidity-free ADHD. The only study that examined a comparable ADHD-pure cohort versus TDC

also observed higher FA with TBSS in those tracts [Silk et al., 2009b]. Their analysis of diffusion eigenvalues within significant FA clusters in the right occipito-parietal and left fronto-temporal cortex generally found higher diffusion in the primary direction accompanied by lower diffusion in the secondary and tertiary directions. This was interpreted as markers of reduced neuronal branching. On the contrary, our observation of higher $K_{||}$ implies increased microstructural complexity as detected by diffusion parallel to axons, which may reflect additional oblique axon collaterals, neuroglial cell membranes, or axonal transport proteins [Wu and Cheung, 2010]. These properties may characterize less refined neural networks owing to inefficient axonal pruning and synaptic refinement [Acebes and Ferrus, 2000]. No group differences in radial metrics were identified, suggesting that axonal integrity/organization may be compromised in the ADHD-pure subgroup rather than myelin integrity. Without specific histological studies, alternative interpretations cannot be excluded because of the limited information provided by diffusion metrics.

As with our age regression findings, combining the ADHD-pure and ADHD-comorbid subgroups obscured the group differences observed between ADHD-pure and TDC. Compared to TDC, the ADHD-mixed group had the same aberrant WM patterns of higher $K_{||}$ found in the ADHD-pure subgroup but additional regions with higher MK were identified in more widespread regions. Analysis of the ADHD-comorbid subgroup detected only the regions with higher MK observed in the ADHD-mixed group. Similar to our age regression results, specific interpretation of this greater microstructural complexity within the ADHD-comorbid subgroup and the ADHD-mixed group is limited given the diversity of comorbidity types involved. Although the majority of studies investigating tissue microstructure in ADHD have included comorbidity, they have yielded mixed findings of decreased and/or increased FA or MD [Ashtari et al., 2005; Bechtel et al., 2009; Cao et al., 2010; Casey et al., 2007; Chao et al., 2009; Davenport et al., 2010; de Zeeuw et al., 2011, 2012; Dramsdahl et al., 2012; Hamilton et al., 2008; Helpern et al., 2011; Kobel et al., 2010; Li et al., 2010; Makris et al., 2008; Nagel et al., 2011; Pavuluri et al., 2009; Peterson et al., 2011; Qiu et al., 2011; Rusch et al., 2007; Skranes et al., 2007; Tamm et al., 2012; Wang et al., 2012]. Direct comparison to prior studies is difficult, given the vast differences in comorbidity types included across studies. Nonetheless, our findings suggest that ADHD patients with comorbidity also exhibit abnormally greater WM microstructural complexity compared to TDC but with a pattern distinct from the ADHD-pure subgroup.

Although these results implicate distinct brain microstructural markers in ADHD without comorbidity, limitations should be noted. Due to our cross-sectional sampling of subjects, these findings require longitudinal replication to confirm lack of age-related change in GM and WM microstructural complexity within the ADHD-pure

subgroup. Because of the cross-sectional design, we were also unable to determine whether the ADHD symptoms in the ADHD-pure and ADHD-comorbid subgroups differed in terms of age-of-onset, phenomenology, or other clues to differential neurobiological substrates. Furthermore, we could not extrapolate our findings from the ADHD-comorbid subgroup given the wide assortment of comorbid disorders that, taken as a composite, does not represent typical profiles observed in the population. Examination of ADHD with a specific type of comorbid disorder or with disorders that share common dimensional symptoms (e.g., externalizing disorders) may better address specific questions regarding ADHD comorbidity. Additionally, as the ADHD-mixed group ($n = 22$) was divided for subsequent subgroup analyses, statistical power was reduced and compared to analyses of the whole ADHD-mixed cohort and may explain why some regions with age-related changes and group differences in the ADHD-mixed group were not detected in either ADHD subgroup. Still, we note that the lack of age-related change in brain microstructural complexity in the ADHD-pure subgroup was replicated in a separate, predominantly comorbidity-free ADHD cohort [Helpern et al., 2011] in which findings were retained when reanalyzed after excluding comorbid cases. Although our sample size was small, the fact that we observed similar results in two independently obtained cohorts of pure- or almost-pure ADHD and that significant findings had moderate to large effect sizes supports the robustness of our results. Nonetheless, the limited sample size reduced statistical power to examine other potential contributing effects such as medication, subtypes, sex, or specific comorbid conditions. However, the ADHD-pure and ADHD-comorbid subgroups did not differ in medication history, subtype, or sex distribution and participants within each ADHD subgroup were evenly distributed within the examined age range to sufficiently sample age-related changes. We also confirmed there were no significant group and subgroup differences (i.e., TDC vs. ADHD-mixed, TDC vs. ADHD-pure, and TDC vs. ADHD-comorbid) in the signal-to-noise ratio and ghosting signal of $b = 0$ images that would indicate head motion, thus ensuring motion artifacts were not driving our results (Supporting Information Table S2). Although our finding of increased WM microstructural complexity is broadly consistent with the existing studies that examined tissue microstructure in comorbidity-free ADHD cohorts [Konrad et al., 2010; Li et al., 2010; Peterson et al., 2011; Silk et al., 2009b], prior studies detected higher FA, whereas we detected higher $K_{\parallel}$ but were unable to detect FA group differences. We acquired diffusion images with slightly larger voxel size compared to the previous DTI studies. This might have increased the confounding effects of crossing fibers which compromise FA sensitivity. Our age-related FA observations in TDC also demonstrate this reduced FA sensitivity in that well-documented global age-related increases in FA were detected only at subthreshold levels (TFCE $p < 0.09$; Supporting Information Fig. S6: first top row).

CONCLUSIONS

In conclusion, our results highlight the shortcomings of including diverse psychiatric comorbidities in the investigation of tissue microstructure in ADHD. Although aberrant findings have been observed with heterogeneous ADHD cohorts, these may lack clinical specificity, as potentially reflected in conflicting results from prior microstructural studies on ADHD. When we excluded the variable contributions of diverse comorbidities by restricting analyses to an ADHD-pure subgroup, we detected greater tissue microstructural complexity, as compared with TDC, in bilateral frontal and parietal lobes, insula, corpus callosum, right external and internal capsules, and we observed an atypical lack of age-related progression in GM and WM microstructural complexity from ages of 8 to 18 yrs. These results may help provide specific biomarkers for the pure form of ADHD which has been shown to respond optimally with medication [Jensen et al., 2001; Newcorn et al., 2001]. The ability to distinguish this pure subset from the comorbid forms of ADHD, which have been shown to respond to other nonpharmacological treatments [Jensen et al., 2001; Newcorn et al., 2001], could support different treatment options when comorbidity is present. Although an integrative model may better represent the complex nature of comorbidity in ADHD, future studies may benefit from systematically examining specific ADHD subsets, comorbidity-free, or with specific types of comorbidities, to explore the possibility of distinct neuro-microstructural correlates. Such investigations could assist in better diagnosis and help guide optimal treatment.

ACKNOWLEGMENTS

REFERENCES

Acebes A, Ferrus A (2000): Cellular and molecular features of axon collaterals and dendrites. Trends Neurosci 23:557–565.

Alexander AL, Lee JE, Lazar M, Field AS (2007): Diffusion tensor imaging of the brain. Neurotherapeutics 4:316–329.

American Psychiatric Association (2000): Diagnostic and Statistical Manual of Mental Disorders, Fourth Edition, Text Revision.

Ashtari M, Kumra S, Bhaskar SL, Clarke T, Thaden E, Cervellione KL, Rhinewine J, Kane JM, Adesman A, Milanaik R, Maytal J,

Diamond A, Szeszko P, Ardekani BA (2005): Attention-deficit-hyperactivity disorder: A preliminary diffusion tensor imaging study. Biol Psychiatry 57:448–455.

Baumgardner TL, Singer HS, Denckla MB, Rubin MA, Abrams MT, Colli MJ, Reiss AL (1996): Corpus callosum morphology in children with Tourette syndrome and attention deficit hyperactivity disorder. Neurology 47:477–482.

Bava S, Thayer R, Jacobus J, Ward M, Jernigan TL, Tapert SF (2010): Longitudinal characterization of white matter maturation during adolescence. Brain Res 1327:38–46.

Bechtel N, Kobel M, Penner IK, Klarhofer M, Scheffler K, Opwis K, Weber P (2009): Decreased fractional anisotropy in the middle cerebellar peduncle in children with epilepsy and/or attention deficit/hyperactivity disorder: A preliminary study. Epilepsy Behav 15:294–298.

Benes FM, Turtle M, Khan Y, Farol P (1994): Myelination of a key relay zone in the hippocampal formation occurs in the human brain during childhood, adolescence, and adulthood. Arch Gen Psychiatry 51:477–484.

Blockx I, De Groof G, Verhoye M, Van Audekerke J, Raber K, Poot D, Sijbers J, Osmand AP, Von Horsten S, Van der Linden A (2012a): Microstructural changes observed with DKI in a transgenic Huntington rat model: Evidence for abnormal neurodevelopment. Neuroimage 59:957–967.

Blockx I, Verhoye M, Van Audekerke J, Bergwerf I, Kane JX, Delgado Y Palacios R, Veraart J, Jeurissen B, Raber K, von Horsten S, Ponsaerts P, Sijbers J, Leergaard TB, Van der Linden A (2012b): Identification and characterization of Huntington related pathology: An in vivo DKI imaging study. Neuroimage 63:653–662.

Cao Q, Sun L, Gong G, Lv Y, Cao X, Shuai L, Zhu C, Zang Y, Wang Y (2010): The macrostructural and microstructural abnormalities of corpus callosum in children with attention deficit/hyperactivity disorder: A combined morphometric and diffusion tensor MRI study. Brain Res 1310:172–180.

Casey BJ, Epstein JN, Buhle J, Liston C, Davidson MC, Tonev ST, Spicer J, Niogi S, Millner AJ, Reiss A, Garrett A, Hinshaw SP, Greenhill LL, Shafritz KM, Vitolo A, Kotler LA, Jarrett MA, Glover G (2007): Frontostriatal connectivity and its role in cognitive control in parent-child dyads with ADHD. Am J Psychiatry 164:1729–1736.

Chao TC, Chou MC, Yang P, Chung HW, Wu MT (2009): Effects of interpolation methods in spatial normalization of diffusion tensor imaging data on group comparison of fractional anisotropy. Magn Reson Imaging 27:681–690.

Cheung JS, Wang E, Lo EH, Sun PZ (2012): Stratification of heterogeneous diffusion MRI ischemic lesion with kurtosis imaging: evaluation of mean diffusion and kurtosis MRI mismatch in an animal model of transient focal ischemia. Stroke 43:2252–2254.

Cheung MM, Hui ES, Chan KC, Helpern JA, Qi L, Wu EX (2009): Does diffusion kurtosis imaging lead to better neural tissue characterization? A rodent brain maturation study. Neuroimage 45:386–392.

Conners CK (1997a/b): Conners' Rating Scales-Revised Technical-User's Manual.

Davenport ND, Karatekin C, White T, Lim KO (2010): Differential fractional anisotropy abnormalities in adolescents with ADHD or schizophrenia. Psychiatry Res 181:193–198.

de Zeeuw P, Mandl RC, Hulshoff Pol HE, van Engeland H, Durston S (2011): Decreased frontostriatal microstructural organization in attention deficit/hyperactivity disorder. Hum Brain Mapp 33:1941–1951.

de Zeeuw P, Schnack HG, van Belle J, Weusten J, van Dijk S, Langen M, Brouwer RM, van Engeland H, Durston S (2012): Differential brain development with low and high IQ in attention-deficit/hyperactivity disorder. PLoS One 7:e35770.

Dramsdahl M, Westerhausen R, Haavik J, Hugdahl K, Plessen KJ (2012): Adults with attention-deficit/hyperactivity disorder—A diffusion-tensor imaging study of the corpus callosum. Psychiatry Res 201:168–173.

Falangola MF, Jensen JH, Babb JS, Hu C, Castellanos FX, Di Martino A, Ferris SH, Helpern JA (2008): Age-related non-Gaussian diffusion patterns in the prefrontal brain. J Magn Reson Imaging 28:1345–1350.

Gallichan D, Scholz J, Bartsch A, Behrens TE, Robson MD, Miller KL (2010): Addressing a systematic vibration artifact in diffusion-weighted MRI. Hum Brain Mapp 31:193–202.

Gao Y, Zhang Y, Wong CS, Wu PM, Zhang Z, Gao J, Qiu D, Huang B (2012): Diffusion abnormalities in temporal lobes of children with temporal lobe epilepsy: A preliminary diffusional kurtosis imaging study and comparison with diffusion tensor imaging. NMR Biomed 25:1369–1377.

Gioia GA, Isquith PK, Guy SC, Kenworthy L (2000): Behavior rating inventory of executive function. Child Neuropsychol 6:235–238.

Grinberg F, Ciobanu L, Farrher E, Shah NJ (2012): Diffusion kurtosis imaging and log-normal distribution function imaging enhance the visualisation of lesions in animal stroke models. NMR Biomed 25:1295–1304.

Grossman EJ, Ge Y, Jensen JH, Babb JS, Miles L, Reaume J, Silver JM, Grossman RI, Inglese M (2011): Thalamus and cognitive impairment in mild traumatic brain injury: A diffusional kurtosis imaging study. J Neurotrauma 29:2318–2327.

Hamilton LS, Levitt JG, O'Neill J, Alger JR, Luders E, Phillips OR, Caplan R, Toga AW, McCracken J, Narr KL (2008): Reduced white matter integrity in attention-deficit hyperactivity disorder. Neuroreport 19:1705–1708.

Helpern JA, Adisetiyo V, Falangola MF, Hu C, Di Martino A, Williams K, Castellanos FX, Jensen JH (2011): Preliminary evidence of altered gray and white matter microstructural development in the frontal lobe of adolescents with attention-deficit hyperactivity disorder: A diffusional kurtosis imaging study. J Magn Reson Imaging 33:17–23.

Hui ES, Du F, Huang S, Shen Q, Duong TQ (2012): Spatiotemporal dynamics of diffusional kurtosis, mean diffusivity and perfusion changes in experimental stroke. Brain Res 1451:100–109.

Huttenlocher PR, Dabholkar AS (1997): Regional differences in synaptogenesis in human cerebral cortex. J Comp Neurol 387:167–178.

Jensen JH, Helpern JA (2003): Quantifying non-Gaussian water diffusion by means of pulsed-field-gradient MRI. Proc Intl Soc Magn Reson Med 11:2154.

Jensen JH, Helpern JA (2010): MRI quantification of non-Gaussian water diffusion by kurtosis analysis. NMR Biomed 23:698–710.

Jensen JH, Helpern JA, Ramani A, Lu H, Kaczynski K (2005): Diffusional kurtosis imaging: The quantification of non-Gaussian water diffusion by means of magnetic resonance imaging. Magn Reson Med 53:1432–1440.

Jensen JH, Falangola MF, Hu C, Tabesh A, Rapalino O, Lo C, Helpern JA (2011): Preliminary observations of increased diffusional kurtosis in human brain following recent cerebral infarction. NMR Biomed 24:452–457.

Jensen PS, Hinshaw SP, Kraemer HC, Lenora N, Newcorn JH, Abikoff HB, March JS, Arnold LE, Cantwell DP, Conners CK,

Elliott GR, Greenhill LL, Hechtman L, Hoza B, Pelham WE, Severe JB, Swanson JM, Wells KC, Wigal T, Vitiello B (2001): ADHD comorbidity findings from the MTA study: Comparing comorbid subgroups. J Am Acad Child Adolesc Psychiatry 40:147–158.

Jones DK, Knösche TR, Turner R (2013): White matter integrity, fiber count, and other fallacies: The do's and don'ts of diffusion MRI. Neuroimage 73:239–254.

Kaufman J, Birmaher B, Brent D, Rao U, Flynn C, Moreci P, Williamson D, Ryan N (1997): Schedule for Affective Disorders and Schizophrenia for School-Aged Children: Present and Lifetime Version (K-SADS-PL): Initial reliability and validity data. J Am Acad Child Adolesc Psychiatry 36:980–988.

Kobel M, Bechtel N, Specht K, Klarhofer M, Weber P, Scheffler K, Opwis K, Penner IK (2010): Structural and functional imaging approaches in attention deficit/hyperactivity disorder: Does the temporal lobe play a key role? Psychiatry Res 183:230–236.

Konrad K, Eickhoff SB (2010): Is the ADHD brain wired differently? A review on structural and functional connectivity in attention deficit hyperactivity disorder. Hum Brain Mapp 31:904–916.

Konrad A, Dielentheis TF, El Masri D, Bayerl M, Fehr C, Gesierich T, Vucurevic G, Stoeter P, Winterer G (2010): Disturbed structural connectivity is related to inattention and impulsivity in adult attention deficit hyperactivity disorder. Eur J Neurosci 31:912–919.

Konrad A, Dielentheis TF, Masri DE, Dellani PR, Stoeter P, Vucurevic G, Winterer G (2011): White matter abnormalities and their impact on attentional performance in adult attention-deficit/hyperactivity disorder. Eur Arch Psychiatry Clin Neurosci 262:351–360.

Lebel C, Walker L, Leemans A, Phillips L, Beaulieu C (2008): Microstructural maturation of the human brain from childhood to adulthood. Neuroimage 40:1044–1055.

Li Q, Sun J, Guo L, Zang Y, Feng Z, Huang X, Yang H, Lv Y, Huang M, Gong Q (2010): Increased fractional anisotropy in white matter of the right frontal region in children with attention-deficit/hyperactivity disorder: A diffusion tensor imaging study. Neuro Endocrinol Lett 31:747–753.

Lu H, Jensen JH, Ramani A, Helpern JA (2006): Three-dimensional characterization of non-gaussian water diffusion in humans using diffusion kurtosis imaging. NMR Biomed 19:236–247.

Makris N, Buka SL, Biederman J, Papadimitriou GM, Hodge SM, Valera EM, Brown AB, Bush G, Monuteaux MC, Caviness VS, Kennedy DN, Seidman LJ (2008): Attention and executive systems abnormalities in adults with childhood ADHD: A DT-MRI study of connections. Cereb Cortex 18:1210–1220.

Nagel BJ, Bathula D, Herting M, Schmitt C, Kroenke CD, Fair D, Nigg JT (2011): Altered white matter microstructure in children with attention-deficit/hyperactivity disorder. J Am Acad Child Adolesc Psychiatry 50:283–292.

Newcorn JH, Halperin JM, Jensen PS, Abikoff HB, Arnold LE, Cantwell DP, Conners CK, Elliott GR, Epstein JN, Greenhill LL, Hechtman L, Hinshaw SP, Hoza B, Kraemer HC, Pelham WE, Severe JB, Swanson JM, Wells KC, Wigal T, Vitiello B (2001): Symptom profiles in children with ADHD: Effects of comorbidity and gender. J Am Acad Child Adolesc Psychiatry 40:137–146.

Nichols TE, Holmes AP (2002): Nonparametric permutation tests for functional neuroimaging: A primer with examples. Hum Brain Mapp 15:1–25.

Oldfield RC (1971): The assessment and analysis of handedness: The Edinburgh inventory. Neuropsychologia 9:97–113.

Pavuluri MN, Yang S, Kamineni K, Passarotti AM, Srinivasan G, Harral EM, Sweeney JA, Zhou XJ (2009): Diffusion tensor imaging study of white matter fiber tracts in pediatric bipolar disorder and attention-deficit/hyperactivity disorder. Biol Psychiatry 65:586–593.

Peterson DJ, Ryan M, Rimrodt SL, Cutting LE, Denckla MB, Kaufmann WE, Mahone EM (2011): Increased regional fractional anisotropy in highly screened attention-deficit hyperactivity disorder (ADHD). J Child Neurol 26:1296–1302.

Qiu MG, Ye Z, Li QY, Liu GJ, Xie B, Wang J (2011): Changes of brain structure and function in ADHD children. Brain Topogr 24:243–252.

Raab P, Hattingen E, Franz K, Zanella FE, Lanfermann H (2010): Cerebral gliomas: Diffusional kurtosis imaging analysis of microstructural differences. Radiology 254:876–881.

Rosenkrantz AB, Sigmund EE, Johnson G, Babb JS, Mussi TC, Melamed J, Taneja SS, Lee VS, Jensen JH (2012): Prostate cancer: Feasibility and preliminary experience of a diffusional kurtosis model for detection and assessment of aggressiveness of peripheral zone cancer. Radiology 264:126–135.

Rubio B, Hernandez S, Verche E, Martin R, Gonzalez-Perez P (2011): A pilot study: Differential effects of methylphenidate-OROS on working memory and attention functions in children with attention-deficit/hyperactivity disorder with and without behavioural comorbidities. Atten Defic Hyperact Disord 3:13–20.

Rusch N, Weber M, Il'yasov KA, Lieb K, Ebert D, Hennig J, van Elst LT (2007): Inferior frontal white matter microstructure and patterns of psychopathology in women with borderline personality disorder and comorbid attention-deficit hyperactivity disorder. Neuroimage 35:738–747.

Sauder CL, Beauchaine TP, Gatzke-Kopp LM, Shannon KE, Aylward E (2012): Neuroanatomical correlates of heterotypic comorbidity in externalizing male adolescents. J Clin Child Adolesc Psychol 41:346–352.

Silk TJ, Vance A, Rinehart N, Bradshaw JL, Cunnington R (2009a): Structural development of the basal ganglia in attention deficit hyperactivity disorder: A diffusion tensor imaging study. Psychiatry Res 172:220–225.

Silk TJ, Vance A, Rinehart N, Bradshaw JL, Cunnington R (2009b): White-matter abnormalities in attention deficit hyperactivity disorder: A diffusion tensor imaging study. Hum Brain Mapp 30:2757–2765.

Skranes J, Vangberg TR, Kulseng S, Indredavik MS, Evensen KA, Martinussen M, Dale AM, Haraldseth O, Brubakk AM (2007): Clinical findings and white matter abnormalities seen on diffusion tensor imaging in adolescents with very low birth weight. Brain 130:654–666.

Smith SM, Nichols TE (2009): Threshold-free cluster enhancement: Addressing problems of smoothing, threshold dependence and localisation in cluster inference. Neuroimage 44:83–98.

Smith SM, Jenkinson M, Johansen-Berg H, Rueckert D, Nichols TE, Mackay CE, Watkins KE, Ciccarelli O, Cader MZ, Matthews PM, Behrens TE (2006): Tract-based spatial statistics: Voxelwise analysis of multi-subject diffusion data. Neuroimage 31:1487–1505.

Song SK, Sun SW, Ramsbottom MJ, Chang C, Russell J, Cross AH (2002): Dysmyelination revealed through MRI as increased radial (but unchanged axial) diffusion of water. Neuroimage 17:1429–1436.

Tabesh A, Jensen JH, Ardekani BA, Helpern JA (2011): Estimation of tensors and tensor-derived measures in diffusional kurtosis imaging. Magn Reson Med 65:823–836.

Takeda T, Ambrosini PJ, deBerardinis R, Elia J (2012): What can ADHD without comorbidity teach us about comorbidity? Res Dev Disabil 33:419–425.

Tamm L, Barnea-Goraly N, Reiss AL (2012): Diffusion tensor imaging reveals white matter abnormalities in Attention-Deficit/Hyperactivity Disorder. Psychiatry Res 202:150–154.

Van Cauter S, Veraart J, Sijbers J, Peeters RR, Himmelreich U, De Keyzer F, Van Gool SW, Van Calenbergh F, De Vleeschouwer S, Van Hecke W, Sunaert S (2012): Gliomas: Diffusion kurtosis MR imaging in grading. Radiology 263:492–501.

Veraart J, Poot DH, Van Hecke W, Blockx I, Van der Linden A, Verhoye M, Sijbers J (2011): More accurate estimation of diffusion tensor parameters using diffusion Kurtosis imaging. Magn Reson Med 65:138–145.

Wang JJ, Lin WY, Lu CS, Weng YH, Ng SH, Wang CH, Liu HL, Hsieh RH, Wan YL, Wai YY (2011): Parkinson disease: Diagnostic utility of diffusion kurtosis imaging. Radiology 261:210–217.

Wang Y, Horst KK, Kronenberger WG, Hummer TA, Mosier KM, Kalnin AJ, Dunn DW, Mathews VP (2012): White matter abnormalities associated with disruptive behavior disorder in adolescents with and without attention-deficit/hyperactivity disorder. Psychiatry Res 202:245–251.

Webster MJ, Elashoff M, Weickert CS (2011): Molecular evidence that cortical synaptic growth predominates during the first decade of life in humans. Int J Dev Neurosci 29:225–236.

Wechsler D (1999): Wechsler Abbreviated Scale of Intelligence (WASI).

Wu EX, Cheung MM (2010): MR diffusion kurtosis imaging for neural tissue characterization. NMR Biomed 23:836–848.

Zhuo J, Xu S, Proctor JL, Mullins RJ, Simon JZ, Fiskum G, Gullapalli RP (2012): Diffusion kurtosis as an in vivo imaging marker for reactive astrogliosis in traumatic brain injury. Neuroimage 59:467–477.